AIRBORNE RETRIEVAL OF CLOUD PARTICLE SIZE AND WATER CONTENT BY A W-BAND RADAR AND MID-INFRARED LIDAR

David M. Tratt and Robert T. Menzies

Laser Remote Sensing Group

Jet Propulsion Laboratory

Pasadena, CA 91109

Gregory A. Sadowy

Microwave Remote Sensing Laboratory

Dept. of Electrical and Computer Engineering

University of Massachusetts

Amherst, MA 01002

(February 1998)

ABSTRACT

Contemporaneous measurements of cloud backscatter by a W-band radar and a mid-infrared coherent lidar have been conducted from an airborne platform. The effectiveness of this technique for the retrieval of stratiform cloud particle radius information is demonstrated with reference to several case studies. Cloud properties deduced in this manner are evaluated against those derived from analysis of the lidar data in isolation and the relative merits and disadvantages of the combined radar/lidar approach are discussed in relation to experimental findings.

1. Introduction

Full characterization of cloud features and their associated radiative properties is vital to improving our understanding of global climate change processes in so far as these are influenced by mechanisms such as cloud radiative forcing and feedback (Dept. of Energy, 1990).Along with the water content, the effective particle radius is a benchmark parameter in the context of cloud microphysical phenomenology (e.g., Ackerman and Stephens 1987; Hu and Stamnes 1993), so that several approaches have been evolved for the remote determination of this property. Because of the desirability of knowing this information on a global scale, significant efforts have been devoted to retrieval of size parameters from satellite measurements of radiometrically-derived radiances and optical depth (e.g., Minnis *et al.* 1993; Luo *et al.* 1994; Han *et al.* 1994; Kleespies 1995). However, passive measurements of this type are unable to reveal details of multilayer cloud systems or to provide the desired altitude assignments and resolution, so that attention has been directed in recent years to the capabilities of active systems.

Recently, several lidar approaches have been developed to address the issue of particle sizing in clouds. Analysis of multiple scattering angular dependence measurements in the near-infrared have demonstrated high-accuracy size retrieval capability (Benayahu *et al.* 1995), but the constraints placed on the required lidar viewing geometry (<30° elevation angle; oblique view to target cloud formation) may be limiting in certain instances. Platt and Takashima (1987) recognized that in the 9-11 μm spectral region the expression for liquid cloud backscatter-to-extinction ratio reduced to a simple function of the droplet radius. Based on this formulation Eberhard (1993) subsequently

conducted further analytical and experimental studies from a ground-based vantage point, while Menzies *et al.* (1994) applied a variant of the technique to retrieve cloud droplet radii in an airborne context. However, this approach is limited to moderate droplet sizes and is subject to large retrieval errors as one approaches the large radius validity limit (see Section 4).

Inversion of radar reflectance profiles to yield estimates of cloud liquid water content (LWC) and droplet effective radius has been applied in the past with moderate success (e.g., Gossard 1994; Clothiaux *et al.* 1995; Gossard *et al.* 1997; Fox and Illingworth 1997). Because droplet sizes in non-precipitating clouds are much less than the radar wavelength (so that by corollary one is operating within the Rayleigh scattering limit) the implicit assumption frequently made is that there exists a unique and relatively simple equivalence between cloud reflectance and characteristic droplet size (*via* the sixth moment of the droplet size distribution). However, significant scatter has been observed in retrievals obtained through this process which has been linked to the additional dependence on LWC (Atlas *et al.* 1995; Matrosov *et al.* 1995). Improved droplet size retrieval accuracy is achievable if the radar reflectance data are augmented with analogous data obtained by a colocated lidar system (operating at a much shorter wavelength than that of the radar and thus affording very broad spectral separation between the two measurements). Hence there has been a movement in recent years toward combining radar and lidar methods into a cloud sensor system more comprehensive in scope and capability. In the recent past there have been limited exploratory exercises in combining colocated radar and lidar cloud scattering measurements to infer knowledge of the particle microphysics. The first intensive study of this type was conducted during the Cloud Lidar And Radar Exploratory Test (CLARET) field operation in the fall of 1989 and spring of 1991

(Intrieri *et al.* 1993), with subsequent studies being carried out during FIRE II the following fall (Intrieri *et al.* 1995; Matrosov *et al.* 1995). The former campaign demonstrated that the technique could provide cirrus particle size information in good agreement with *in situ* measurements, with the caveat that discrepancies could be expected due to the non-sphericity of the ice particles. However, and in respect of this, one particularly useful feature of the combination radar/lidar technique is the relative robustness of effective particle radius retrieval with respect to measurement imprecision in either the radar or lidar backscatter (Intrieri *et al.* 1993).

These seminal studies involved cirrus targets of large particle size (effective radii 70-200 μm), for which the sensitivity offered by the shortest wavelength radar used (8.6 mm; K_a-band) was adequate. In order to extend the applicability of mm-wave radar into the non-precipitating liquid phase cloud regime it is necessary to take advantage of the increased sensitivity to smaller particles (effective radius <30 μm) afforded by shorter wavelength 3.2- and 1.4-mm systems (e.g., Lhermitte 1987; Mead *et al.* 1989; Sassen and Liao 1996). This paper describes the results of a preliminary study combining cloud backscatter data acquired simultaneously by a 95-GHz (3.2 mm; W-band) radar and a 10.6-μm infrared CO_2 Doppler lidar, both of which were operated in an airborne setting. Case studies under several different conditions are presented which testify to both the strengths and the limitations of this approach to cloud characterization.

2. Field Measurement Considerations

In the summer of 1996 a 95-GHz (3.2-mm) W-band cloud radar (Sadowy *et al.* 1997) and a 10.6-μm infrared Doppler wind lidar (MACAWS; Multi-center Airborne Coherent Atmospheric Wind Sensor [Rothermel *et al.* 1998]) were deployed aboard the NASA DC-8 research aircraft. Although the primary focus of the lidar is the measurement of wind fields, radiometric calibration of the instrument permits the retrieval of atmospheric backscatter cross-section profiles as a byproduct. The salient instrumental characteristics are given in Table 1.

The JPL/UMass cloud radar and MACAWS instruments were developed and flight-manifested on an independent basis without regard to data intercomparison considerations. As such, the correlative results described in this article owe much to an *ad hoc* confluence of circumstances, not all of which were optimal for the study in question. Specifically, the MACAWS lidar is a side-viewing, scanning instrument, while for the summer 1996 flight series the radar was operated in a nadir-staring configuration. The minimum nadir angle view in level flight afforded by the MACAWS beam scanning system is 60° and is only available when the azimuth setting is fixed abeam of the aircraft (Rothermel *et al.* 1997; this was the configuration for all the cases considered in this paper). This limitation meant that at any one time the lidar and radar could not simultaneously target the same atmospheric measurement volume. In order to circumvent this drawback the measures adopted involved traversing a given flight track segment at least twice in opposite directions, so that the lidar would record the backscatter from both flanks of the nadir track while the radar probed the cloud deck in the nadir field-of-regard. If the airborne observers visually identified cloud layers of

sufficient horizontal homogeneity and extent, and if both the radar backscatter profiles agreed and the two lidar profiles showed consistency also, then this provided sufficient evidence of target uniformity to justify proceeding with a data intercomparison. Further corroboration could also be obtained by viewing video camera records of the scene which were acquired as a matter of course during all flights. Clearly, such a strategy is constrained to homogeneous, stratiform cloud systems of large areal extent. The DC-8 flights encountered several cloud systems of this nature which are treated as individual test cases here.

3. Retrieval of Effective Particle Radius from Dual-Wavelength Backscatter Data

(a) Liquid water clouds

Liquid-phase cloud droplet distributions are most commonly described by a modified gamma functional form (e.g., Deirmendjian 1969; Hansen 1971):

$$n(r) = N_0 \left[(r_e b)^{[1-2b]/b} \, \Gamma\left(\frac{1-2b}{b}\right) \right]^{-1} r^{(1-3b)/b} \exp\left(-\frac{r}{r_e b}\right) , \qquad (1)$$

where N_0 is the volumetric droplet total number density, b is the distribution effective variance, and $n(r)$ represents the size distribution function (i.e., the droplet number density *per* unit radius interval at radius r). r_e is the effective droplet radius, defined as:

$$r_e = \frac{\int n(r) r^3 dr}{\int n(r) r^2 dr} . \qquad (2)$$

However, good agreement with measured droplet size spectra has also been reported using the lognormal distribution (Gossard 1994; Gerber 1996):

$$n(r) = \frac{N_0}{r\ln\sigma\sqrt{2\pi}} \exp-\left(\frac{\ln r - \ln r_m}{\sqrt{2}\ln\sigma}\right)^2 , \qquad (3)$$

in which σ is the geometric standard deviation and r_m is the mode (geometric mean) droplet radius:

$$r_m = r_e \exp(-2.5\ln^2\sigma). \qquad (4)$$

The dispersion parameters for these two forms are related through the equivalence:

$$b = \exp(\ln^2\sigma) - 1. \qquad (5)$$

Although the focus here on r_e minimizes the retrieval sensitivity toward the distribution shape and variance, these factors nevertheless introduce a residual uncertainty in the inferred values of r_e. Terrestrial liquid cloud parameterization schemes (Hansen 1971; Chýlek *et al.* 1992) recognize a canonical droplet size variance range of $0.1 \le b \le 0.2$ (and therefore by corollary: $1.35 \le \sigma \le 1.55$). An additional source of uncertainty also results from the non-negligible temperature dependence of the complex refractive index for water in the 95-GHz spectral region. Of these, the temperature accounts for 30-40% spread in the backscatter ratio, while the effect due to size distribution form function was found to be negligible, in agreement with Gossard (1994). The largest contribution to the retrieval error (~300% spread in backscatter ratio) arises from the uncertainty in size distribution variance. Figure 1 comprises modeled Mie scattering predictions of the β[3.2-mm]/β[10.6-μm] backscatter ratio as a function of r_e. The finite breadth of the Mie solution space (i.e., the area bounded by the two curves in Fig. 1) incorporates the range of distribution parameters listed above as computed for the nominal temperature extrema of atmospheric liquid water ($-10°C \le T \le +30°C$). This solution space is well approximated by the following empiricism:

$$r_e = (94 \pm 11\mu m)\left(\frac{\beta[3.2-mm]}{\beta[10.6-\mu m]}\right)^{0.24}_{water} \quad . \qquad (2 \le r_e[\mu m] \le 200) \qquad (6)$$

The range of validity given for this relation encompasses virtually all classes of water cloud from fog to light drizzle. Assuming precise knowledge of the radar/lidar backscatter ratio, therefore, the value of r_e may be inferred within a confidence interval of ~23%. (In passing, we may note here the fourth-root dependence of r_e upon β, which explains the insensitivity of the combined lidar/radar technique toward measurement imprecision in the backscatter measurements to which Intrieri *et al.* (1993) refer. This dependence is transparent from an intuitive viewpoint, since it derives from a convolution of the $\beta \propto r^6$ behavior of the Rayleigh scattering limit appropriate to the radar signal with that of the $\beta \propto r^2$ characteristic of the Mie scattering dominated lidar signal.)

The foregoing discussion has assumed knowledge of the true (i.e., unattenuated) backscatter coefficients involved. At 95 GHz the attenuation within a non-precipitating cloud is small (~0.2 dB km^{-1} [Lhermitte 1988]) and may effectively be ignored in the present application scenario. However, this is not the case in the 9-11 μm mid-infrared spectral region, so that further measures are necessary in order to extract true backscatter coefficients from the *attenuated* backscatter coefficient data (β_a) obtained by the lidar.

The cloud volume extinction coefficient α can be estimated to first order by assuming a constant $\alpha = \beta_a / k$ (where k is as defined in the next section) for the cloud deck and applying this knowledge to infer an intermediate, partially attenuation-compensated backscatter coefficient β':

$$\beta' = \frac{\beta_a}{1 - \exp(-2\alpha\Delta R)} \quad , \qquad (7)$$

in which ΔR represents the penetration distance into the cloud. For the present study we elected to intercompare the peak backscatter values from the cloud feature, so that an appropriate value for ΔR was chosen based on inspection of the lidar data. The intermediate backscatter β' thus generated can then be used to derive an improved value for α and the process iterated to the point where an adequately precise estimate for the true backscatter β has been reached. In practice, the iteration procedure was terminated when the incremental change in β' did not exceed 1%.

(b) Cirrus

The treatment of cirrus is a considerably less tractable procedure because of the variegated habits and orientations that ice crystals can assume. Recognizing that this compromises the applicability of Mie scattering theory in the context of ice clouds we have nevertheless opted to use the Mie approach due to a lack of any specific knowledge of the crystal ensemble prevailing within our target cloud systems. As such, we are then assuming that the cirrus cloud comprises a distribution of ice spherules.

In natural cirrus formations there is an observed tendency for the ice particles to align with their major dimension oriented in the horizontal. Considerable effort has been expended in the assessment of orientational effects in the mm-wave (e.g., Matrosov 1991; Schneider and Stephens 1995) and optical (e.g., Rockwitz 1989; Macke 1993) spectral regions. Experimental observations of particle alignment induced depolarization at 95 GHz were made during an earlier deployment of a similar

radar system (Galloway *et al.* 1997), but the total effective backscatter is only weakly dependent on particle orientation and is muted further still the deeper one penetrates into the Rayleigh scattering regime (Tang and Aydin 1995). By contrast, in the mid-infrared the preferred horizontal orientation of cirrus platelets has been shown to dramatically enhance lidar returns through the addition of a quasi-specular reflection component to the backscatter signal (Platt 1978; Platt *et al.* 1978). It is in this latter regard that the 60° nadir viewing geometry of the MACAWS lidar presents an advantage to this study, in that this incidence angle means that the quasi-specular contribution (which decreases much more rapidly with incidence angle than does the Lambertian component) is effectively eliminated from the return (Platt *et al.* 1978). In addition, the oblique viewing angle will also tend to reduce the effective particle area presented to the lidar to a value closer to the "equal volume spherical equivalent" and can be expected to aid in the retrieval of more realistic estimates for r_e.

Dowling and Radke (1990) have pointed out that the extremely broad ranges evinced by the microphysical properties of natural cirrus resist their easy description by analytical formulæ. Furthermore, where systematic measurements are available, size distributions are frequently characterized by a high incidence of bimodality (Heymsfield 1975; Arnott *et al.* 1994; Mitchell *et al.* 1996). Notwithstanding this obstacle, Kosarev and Mazin (1991) analyzed an extensive cirrus database originated in the former USSR and concluded that most occurrences could be well represented on the local scale by a summation of zeroth (i.e., exponential) and first order gamma distributions. This is frequently truncated to just the first order component in many of the published studies, while others have invoked a broader interpretation which includes a second order gamma term (e.g., Atlas *et al.* 1995; Schneider and Stephens 1995). We have favored the latter policy here

by selecting orders 0 - 2 (or $0.20 \leq b \leq 0.33$ in the nomenclature of Eq. [1]) for the modified gamma size distribution used to generate Figure 2. This display is analogous to Figure 1, but with ice substituted for water in the Mie scattering algorithm so that the resulting solution space is described by the following representation:

$$r_e = (112 \pm 8\mu m) \left(\frac{\beta[3.2-mm]}{\beta[10.6-\mu m]} \right)^{0.25}_{ice} , \qquad (r_e \leq 120\mu m) \qquad (8)$$

in which β is again the true, attenuation-compensated backscatter coefficient.

4. Retrieval of Effective Droplet Radius from Mid-Infrared Backscatter Data

It has been noted that the phenomenology of water cloud optical properties in the thermal infrared spectral region can provide a simple means of characterizing droplet size (Platt and Takashima 1987). This premise is based on the following observation:

$$\int_{cloud} \beta_a(\pi,R)dR = \frac{k}{2\eta} [1 - \exp(-2\eta\delta)] , \qquad (9)$$

where β_a is the range-dependent backscatter uncorrected for in-cloud attenuation (the so-called *attenuated backscatter coefficient*, which is a lidar measurable), k is the backscatter-to-extinction ratio (assumed constant throughout the cloud), and δ is the cloud optical depth along the lidar line-of-sight. η accounts for multiple scattering effects suffered by the lidar beam within the cloud; in the case of an airborne thermal infrared lidar employing coherent detection such as MACAWS, it can

be equated to unity (Menzies *et al.* 1994). In the case of an optically thick cloud (such as that featured in the first case study below) the term within square brackets tends to unity.

Figure 3 expresses the dependence of k on droplet radius at the MACAWS operational wavelength (10.6 μm), as derived from Mie theory. Note that the asymptotic behavior of this relationship at larger droplet sizes leads to a radius retrieval limit (as well as somewhat marginal retrieval accuracy), while the bifurcation of the curve for $r_e > 7$ μm connotes the size distribution uncertainties discussed in the previous section. Retrieval of r_e through this means is used in this study to cross-check and validate the r_e estimates obtained by the lidar/radar backscatter intercomparison method.

5. Case Studies

Of the several intercomparison opportunities which resulted from the 1996 flight series, three case studies in particular were chosen in order to illustrate both the merits and the limitations of the combined radar/lidar backscatter technique. In each instance, vertical and horizontal homogeneity of the subject cloud deck were verified using the procedure outlined in Section 2 above. The study results are summarized in Table 2, in which LWC has been estimated according to (Platt and Takashima 1987):

$$LWC = \frac{4\pi\beta[10.6\text{-}\mu m]}{kK} \quad , \qquad (10)$$

where β[10.6-μm] is the true backscatter coefficient (computed in the manner described in Section 3) and K is the mass extinction coefficient. K is substantially independent of droplet size distribution;

at the 10.6-μm MACAWS operating wavelength it takes a value ~0.1375 g^{-1} m^2 (Platt and Takashima 1987).

The peak ice water content (IWC) quoted for case study (c) in Table 2 has been calculated from the radar data using the Atlas *et al.* (1995) formulation which we recast in terms of backscatter coefficient rather than radar reflectance:

$$IWC\ (g\ m^{-3}) = \frac{395}{r_e^{1.9}} \left(\frac{4\times10^{18}\ \lambda^4\ \beta[\lambda]}{\pi^4} \left| \frac{m^2-1}{m^2+2} \right|^{-2} \right) \quad , \qquad (11)$$

where all terms on the RHS are expressed in SI units (except r_e: μm), λ is the radar wavelength, and m is the complex refractive index for ice.

(a) Altocumulus, Arkansas, US, June 24, 1996

On June 24, 1996, the NASA DC-8 overflew a spatially extensive mid-level (4km MSL) altocumulus (Ac) deck present over southern Arkansas. Two flight segments in opposing directions over the same geographical coordinates, acquired some 10 mins. apart, were selected for study. The backscatter profiles obtained by the radar and lidar instruments are shown in Figure 4, from which the degree of homogeneity of the cloud horizon is readily apparent. It is also evident from Fig. 4 that the cloud deck consists for the most part of at least two distinct strata. The backscatter values used for the intercomparison exercise are those appropriate for the uppermost resolved layer.

The computed backscatter ratio, when processed using Eq. (6), implies an average droplet radius r_e $\approx 15.6 \pm 1.8$ μm. The absence of return from either the surface or boundary layer aerosol in the lidar profiles signifies an optically thick cloud; application of the reduced form ($\delta \rightarrow \infty$) of Eq. (9) to the lidar data, followed by comparison against the theoretical curves in Fig. 3, yields $r_e \approx 17.3 \pm 2.3$ μm. In this particular case the convergence of these two separate approaches provides for a useful confidence in the retrieved droplet characteristic size: Typically one would associate somewhat smaller droplets with a cloud of this type (e.g., Chýlek *et al.* 1992; Han *et al.* 1994; Pontikis 1996), although Gerber (1996) has inferred the existence of a threshold for "heavy drizzle" conditions in stratocumulus clouds occurring near $r_e \approx 16$ μm.

(b) Stratocumulus, Texas, US, June 26, 1996

On June 26, 1996, an extensive low-level (2km MSL) stratocumulus (Sc) deck was encountered over northeastern Texas. Two flight segments were again selected for analysis and are illustrated in Figure 5. However, this case study proved to be not so clearcut since, although the lidar time series data indicated a cloud deck of ostensibly uniform density and broad spatial extent, the radar time series contained only sporadic returns from isolated areas. In addition, the dataset indicated the presence of a cirrus layer approximately 1km beneath the aircraft (see Fig. 5). Although in general we might expect the lidar signal to suffer substantial attenuation within cirrus, inspection of neighboring cirrus-free lidar data segments showed that the attenuation suffered on penetrating the subject cirrus formation was negligible, echoing prior findings obtained with a similar airborne lidar system (Menzies and Tratt 1991). The integrated attenuated backscatter procedure therefore remains applicable in this case, although in this case the Sc deck exhibited significant transmittance for the

lidar beam, as is evident from the appearance in Fig. 5(a) of weak surface strikes and partial returns from an underlying scattering layer at 1-km altitude. Examination of neighboring data segments transitioning to cloud-free conditions implied a two-way transmittance of ~10% which, when applied with Eq. (9), yields an $r_e \approx 9.5 \pm 0.5$ μm for the Sc deck during the selected time periods indicated in Fig. 5. Once the true peak backscatter has been computed it is then possible to estimate the equivalent radar backscatter using the inverted form of Eq. (6). The result is β[3.2-mm] ~ 7×10^{-11} m^{-1} sr^{-1}, or -34 dBZ in standard radar reflectance units. This happens to be coincident with the radar sensitivity limit at the nominal 9-km range corresponding to the Sc deck, thus explaining the sporadic nature of the radar returns in this case. The radar backscatter signal, being $\propto r^6$ and near the detectivity threshold, is very sensitive to small variations in r_e, which were evidently extant within the selected time periods but not obvious from either visual or lidar profile observations. Where the radar time series does indicate occasional strong returns from the cloud deck, these often tend to exhibit streaks which extend down to the surface, strongly suggesting that precipitation (and therefore much larger characteristic droplet size) is prevalent in these localized areas. Also discernable from Fig. 5(b) is a stable, well-defined feature beneath the Sc at about 1-km altitude, which likely signifies cloud generated at the boundary layer capping inversion. While this feature is clearly, and reproducibly, captured in the radar data (though only scattered returns can be observed in the time series display), it is not fully or definitively resolved by the lidar because the optical depth of the overlying Sc has by this point substantially attenuated the 10.6-μm radiation.

While it does not provide an opportunity for a radar/lidar backscatter intercomparison, this particular case study is useful for its clear illustration of the limitations adhering to each of the separate sensor

systems used in this study, as well as highlighting their essential complementarity within the context of cloud remote sensing.

(c) Cirrus, Texas, US, June 26, 1996

The cirrus just below flight level referred to in the previous case study is now considered in its own right. Inspection of the time series data identified a region of suitable spatial homogeneity which was traversed in opposite directions with a temporal separation of some 15 mins. The resultant flight track averaged backscatter profiles are depicted in Figure 6. Due to an operational anomaly, the MACAWS intercomparison data for the second pass over the cirrus target were lost, so that Fig. 6(a) represents only the initial traverse. Consistency of the two radar profiles, along with that of the corresponding video scene records, was therefore used to assess the spatial homogeneity requirement necessary for the intercomparison. Reiterating the findings from the foregoing case study, it was determined that this cirrus deck was of sufficiently low optical depth that we are able to neglect any residual attenuation experienced by the lidar beam. (Recent work suggests that this may be due to a conspicuous extinction window, which is particularly pronounced for smaller particles, caused by a resonance in the Christiansen effect in ice near 10.5 μm [Yang *et al.* 1997].) Thus we are in this case justified in applying Eq. (8) throughout the entire depth of the cirrus to generate a range-resolved profile of the retrieved r_e. The result of this process can be viewed in Figure 7, where the solid line represents the nominal inferred effective radius and the broken curves delineate the uncertainty limits given for Eq. (8). The sharp drop in effective radius apparent at the upper and lower boundaries of the data is in all likelihood not real, but rather due to incomplete filling of the sensor range gates at the ceiling and base of the cirrus formation. While the retrieved particle sizes

implied by Fig. 7 are commensurate with the known general properties of cirrus (e.g., Dowling and Radke 1990), it is inappropriate to conclude more concerning this result in the absence of any correlative *in situ* measurements.

6. Conclusion

We have demonstrated that the combined lidar/radar differential backscatter technique for remote determination of cloud parameters, previously implemented only from static ground-based vantage points against cirrus targets, can be operated effectively from an airborne platform to study both liquid water and ice clouds. In particular, the lidar/radar approach can be applied to remotely ascertain the cloud particle effective radius and water content with moderate accuracy. The complementarity of the individual radar and lidar capabilities is illustrated with reference to case studies which both support the practical validity of the lidar/radar technique and also elucidate the atmospheric conditions which bound its applicability.

In the case of liquid water clouds it has been observed that the single largest source of uncertainty in particle size retrieval through this means emanates from lack of knowledge of the size distribution variance. While additional errors accrue when analyzing cirrus clouds by this technique due to the uncertainty in ice crystal shape and orientation, there is nevertheless a useful functionality attaching to the combination radar/lidar scatter method in this application also.

Acknowledgments

Field operation and subsequent data validation for the instrumentation used in this study is an intensive activity involving many individuals and organizations. We therefore gratefully acknowledge our colleagues R. M. Hardesty and J. N. Howell of the NOAA Environmental Technology Lab. (Boulder, Colo.), J. Rothermel, S. C. Johnson, and D. R. Cutten of the NASA Marshall Space Flight Center (Huntsville, Ala.), S. J. Dinardo, S. L. Durden, A. B. Tanner, and A. M. Brothers at JPL, and the DC-8 staff of the NASA Ames Research Center (Moffett Field, Calif.). We also acknowledge technical discussions with T. L. Schneider (Colorado State Univ., Fort Collins) during field operations. The MACAWS and cloud radar programs are supported by Dr. Ramesh Kakar, NASA Office of Mission to Planet Earth. This work was carried out by the Jet Propulsion Laboratory (JPL), California Institute of Technology (Caltech), under contract to the National Aeronautics and Space Administration (NASA), using computing resources provided by the JPL/Caltech Supercomputing Project.

	RADAR	MACAWS
Operating wavelength	**3.2 mm**	**10.6 μm**
Pulse duration	**250, 500, 1000 ns**	**3 μs**
Pulse repetition frequency	**5 - 20 kHz**	**0.1 - 30 Hz**
Beam diameter	**30 cm**	**20 cm (e^{-2})**
Beam full width	**15 mrad (3dB)**	**0.3 mrad**
Range resolution	**38, 75, 150 m**	**150, 300 m**

Table 1. Principle instrument characteristics. The duration given for the lidar pulse (whose profile is not regular) includes both the initial ~500-ns long gain-switched spike as well as the subsequent long-duration tail.

CASE STUDY	β[3.2-mm] (m^{-1} sr^{-1})	β[10.6-μm] (m^{-1} sr^{-1})	r_e (μm) (radar/lidar)	k (sr^{-1})	r_e (μm) (lidar only)	IWC*/LWC ($g\ m^{-3}$)
Southern Arkansas; June 24, 1996 (Ac)	8.4×10^{-10}	1.5×10^{-6}	15.6 ± 1.8	3.13×10^{-4}	17.3 ± 2.3	0.425
Northeast Texas; June 26, 1996 (Sc)	_	1.0×10^{-6}	N/A	5.70×10^{-4}	9.5 ± 0.5	0.164
Northeast Texas; June 26, 1996 (Ci)	3.4×10^{-8}	6.9×10^{-8}	93.8 ± 6.7	_	N/A	0.059*

Table 2. Summary of cloud properties retrieved using the combined radar/lidar scheme compared to those obtained through the lidar-only approach (see text). The value given for β[10.6-μm] is the estimated true (unattenuated) peak backscatter coefficient.

REFERENCES

Ackerman, S. A., and G. L. Stephens, 1987: The absorption of solar radiation by cloud droplets: An application of anomalous diffraction theory. *J. Atmos. Sci.*, **44**(12), 1574-1588.

Arnott, W. P., Y. Dong, J. Hallett, and M. R. Poellot, 1994: Role of small ice crystals in radiative properties of cirrus: A case study, FIRE II, November 22, 1991. *J. Geophys. Res.*, **99**(D1), 1371-1381.

Atlas, D., S. Y. Matrosov, A. J. Heymsfield, M.-D. Chou, and D. B. Wolff, 1995: Radar and radiation properties of ice clouds. *J. Appl. Meteorol.*, **34**(11), 2329-2345.

Benayahu, Y., A. Ben-David, S. Fastig, and A. Cohen, 1995: Cloud-droplet-size distribution from lidar multiple-scattering measurements. *Appl. Opt.*, **34**(9), 1569-1578.

Chýlek, P., P. Damiano, D. Ngo, and R. G. Pinnick, 1992: Polynomial approximation of the optical properties of water clouds in the 8-12-μm spectral region. *J. Appl. Meteorol.*, **31**(10), 1210-1218.

Clothiaux, E. E., M. A. Miller, B. A. Albrecht, T. P. Ackerman, J. Verlinde, D. M. Babb, R. M. Peters, and W. J. Syrett, 1995: An evaluation of a 94-GHz radar for remote sensing of cloud properties. *J. Atmos. Oceanic Technol.*, **12**(2), 201-229.

Deirmendjian, D., 1969: *Electromagnetic Scattering on Spherical Polydispersions*. Elsevier, 290 pp.

Department of Energy, 1990: Atmospheric Radiation Measurement Program. *US Dept. of Energy, Office of Energy Research Technical Report DOE/ER-0441.*

Dowling, D. R., and L. F. Radke, 1990: A summary of the physical properties of cirrus clouds. *J. Appl. Meteorol.*, **29**(9), 970-978.

Eberhard, W. L., 1993: CO_2 lidar technique for observing characteristic drop size in water clouds. *IEEE Trans. Geosci. Remote Sensing*, **31**(1), 56-63.

Fox, N. I., and A. J. Illingworth, 1997: The potential of a spaceborne cloud radar for the detection of stratocumulus clouds. *J. Appl. Meteorol.*, **36**(6), 676-687.

Galloway, J., A. Pazmany, J. Mead, R. E. McIntosh, D. Leon, J. French, R. Kelly, and G. Vali, 1997: Detection of ice hydrometeor alignment using an airborne W-band polarimetric radar. *J. Atmos. Oceanic Technol.*, **14**(4), 3-12.

Gerber, H., 1996: Microphysics of marine stratocumulus clouds with two drizzle modes. *J. Atmos. Sci.*, **53**(12), 1649-1662.

Gossard, E. E., 1994: Measurement of cloud droplet size spectra by Doppler radar. *J. Atmos. Oceanic Technol.*, **11**(3), 712-726.

Gossard, E. E., J. B. Snider, E. E. Clothiaux, B. Martner, J. S. Gibson, R. A. Kropfli, and A. S. Frisch, 1997: The potential of 8-mm radars for remotely sensing cloud drop size distributions. *J. Atmos. Oceanic Technol.*, **14**(1), 76-87.

Han, Q., W. B. Rossow, and A. A. Lacis, 1994: Near-global survey of effective droplet radii in liquid water clouds using ISCCP data. *J. Climate*, **7**(4), 465-497.

Hansen, J. E., 1971: Multiple scattering of polarized light in planetary atmospheres. Part II. Sunlight reflected by terrestrial water clouds. *J. Atmos. Sci.*, **28**(8), 1400-1426.

Heymsfield, A. J., 1975: Cirrus uncinus generating cells and the evolution of cirriform clouds. Part I: Aircraft observations of the growth of the ice phase. *J. Atmos. Sci.*, **32**(4), 799-808.

Hu, Y. X., and K. Stamnes, 1993: An accurate parameterization of the radiative properties of water clouds suitable for use in climate models. *J. Climate*, **6**(4), 728-742.

Intrieri, J. M., W. L. Eberhard, T. Uttal, J. A. Shaw, J. B. Snider, Y. Han, B. W. Orr, and S. Y. Matrosov, 1995: Multiwavelength observations of a developing cloud system: The FIRE II 26 November 1991 case study. *J. Atmos. Sci.*, **52**(23), 4079-4093.

Intrieri, J. M., G. L. Stephens, W. L. Eberhard, and T. Uttal, 1993: A method for determining cirrus cloud particle sizes using lidar and radar backscatter techniques. *J. Appl. Meteorol.*, **32**(6), 1074-1082.

Kleespies, T. J., 1995: The retrieval of marine stratiform cloud properties from multiple observations in the 3.9-μm window under conditions of varying solar illumination. *J. Appl. Meteorol.*, **34**(7), 1512-1524.

Kosarev, A. L., and I. P. Mazin, 1991: An empirical model of the physical structure of upper-layer clouds. *Atmos. Res.*, **26**(3), 213-228.

Lhermitte, R. M., 1987: Small cumuli observed with a 3 mm wavelength Doppler radar. *Geophys. Res. Lett.*, **14**(7), 707-710.

Lhermitte, R. M., 1988: Cloud and precipitation remote sensing at 94 GHz. *IEEE Trans. Geosci. and Remote Sensing*, **26**(3), 207-216.

Lhermitte, R., 1990: Attenuation and scattering of millimeter wavelength radiation by clouds and precipitation. *J. Atmos. Oceanic Technol.*, **7**(3), 464-479.

Luo, G., X. Lin, and J. A. Coakley, Jr., 1994: 11-μm emissivities and droplet radii for marine stratocumulus. *J. Geophys. Res.*, **99**(D2), 3685-3698.

Macke, A., 1993: Scattering of light by polyhedral ice crystals. *Appl. Opt.*, **32**(15), 2780-2788.

Matrosov, S. Y., 1991: Theoretical study of radar polarization parameters obtained from cirrus clouds. *J. Atmos. Sci.*, **48**(8), 1062-1070.

Matrosov, S. Y., 1997: Variability of microphysical parameters in high-altitude ice clouds: Results of the remote sensing method. *J. Appl. Meteorol.*, **36**(6), 633-648.

Matrosov, S. Y., A. J. Heymsfield, J. M. Intrieri, B. W. Orr, and J. B. Snider, 1995: Ground-based remote sensing of cloud particle sizes during the 26 November 1991 FIRE II cirrus case: Comparisons with in situ data. *J. Atmos. Sci.*, **52**(23), 4128-4142.

Mead, J. B., R. E. McIntosh, D. Vandemark, and C. T. Swift, 1989: Remote sensing of clouds and fog with a 1.4-mm radar. *J. Atmos. Oceanic. Technol.*, **6**(6), 1090-1097.

Menzies, R. T., and D. M. Tratt, 1991:Aerosol and cloud observations with a CO_2 backscatter lidar on the NASA DC-8 GLOBE Pacific missions. *Proc. Seventh Symposium on Meteorological Observations and Instrumentation: Laser Atmospheric Studies* (New Orleans, LA), Amer. Meteorol. Soc., Boston, MA, J265-J267.

Menzies, R. T., D. M. Tratt, and P. H. Flamant, 1994: Airborne CO_2 coherent lidar measurements of cloud backscatter and opacity over the ocean surface. *J. Atmos. Oceanic Technol.*, **11**(3), 770-778.

Minnis, P., P. W. Heck, and D. F. Young, 1993: Inference of cirrus cloud properties using satellite-observed visible and infrared radiances. Part II: Verification of theoretical cirrus radiative properties. *J. Atmos. Sci.*, **50**(9), 1305-1322.

Mitchell, D. L., S. K. Chai, Y. Liu, A. J. Heymsfield, and Y. Dong, 1996: Modeling cirrus clouds. Part I: Treatment of bimodal size spectra and case study analysis. *J. Atmos. Sci.*, **53**(20), 2952-2966.

Platt, C. M. R., 1978: Lidar backscatter from horizontal ice crystal plates. *J. Appl. Meteorol.*, **17**(4), 482-488.

Platt, C. M. R., N. L. Abshire, and G. T. McNice, 1978: Some microphysical properties of an ice cloud from lidar observations of horizontally oriented crystals. *J. Appl. Meteorol.*, **17**(8), 1220-1224.

Platt, C. M. R., and T. Takashima, 1987: Retrieval of water cloud properties from carbon dioxide laser soundings. *Appl. Opt.*, **26**(7), 1257-1263.

Pontikis, C. A., 1996: Parameterization of the droplet effective radius of warm layer clouds. *Geophys. Res. Lett.*, **23**(19), 2629-2632.

Rockwitz, K. -D., 1989: Scattering properties of horizontally oriented ice crystal columns in cirrus clouds. Part I. *Appl. Opt.*, **28**(19), 4103-4110.

Rothermel, J., D. R. Cutten, R. M. Hardesty, R. T. Menzies, J. N. Howell, S. C. Johnson, D. M. Tratt, L. D. Olivier, and R. M. Banta, 1998: The Multi-center Airborne Coherent Atmospheric Wind Sensor, MACAWS. *Bull. Amer. Meteorol. Soc.*, **79**(4), (in press)

Sadowy, G. A., R. E. McIntosh, S. J. Dinardo, S. L. Durden, W. N. Edelstein, F. K. Li, A. B. Tanner, W. J. Wilson, T. L. Schneider, and G. L. Stephens, 1997: NASA DC-8 Airborne Cloud Radar: design and preliminary results. *International Geoscience and Remote Sensing Symposium*, Singapore.

Sassen, K., and L. Liao, 1996: Estimation of cloud content by W-band radar. *J. Appl. Meteorol.*, **35**(6), 932-938.

Schneider, T. L., and G. L. Stephens, 1995: Theoretical aspects of modeling backscattering by cirrus ice particles at millimeter wavelengths. *J. Atmos. Sci.*, **52**(23), 4367-4385.

Tang, C., and K. Aydin, 1995: Scattering from ice crystals at 94 and 220 GHz millimeter wave frequencies. *IEEE Trans. Geosci. Remote Sensing*, **33**(1), 93-99.

Yang, P., K. N. Liou, and W. P. Arnott, 1997: Extinction efficiency and single-scattering albedo for laboratory and natural cirrus clouds. *J. Geophys. Res.*, **102**(D18), 21825-21835.

FIGURE CAPTIONS

Figure 1. Mie theory simulations of 3.2-mm/10.6-μm backscatter ratio as a function of water droplet effective radius. The broad solution space derives primarily from the variation in droplet size spectrum observed in natural non-precipitating water clouds.

Figure 2. Mie theory simulations of 3.2-mm/10.6-μm backscatter ratio as a function of ice spherule effective radius. The broad solution space derives from the variation in particle size spectrum observed in natural cirrus clouds.

Figure 3. Dependence of cloud backscatter-to-extinction ratio at $\lambda = 10.6$ μm as a function of water droplet effective radius, as predicted by Mie theory. The bifurcate character of the relation denotes the uncertainty due to variations in the droplet size spectrum observed in natural non-precipitating water clouds.

Figure 4. Backscatter signatures of altocumulus cloud deck (case study, June 24, 1996) averaged over the two flight segment intervals indicated; (a) lidar profiles, (b) radar profiles. Times specified are UTC.

Figure 5. Backscatter signatures of stratocumulus cloud deck (case study, June 26, 1996) averaged over the two flight segment intervals indicated; (a) lidar profiles, (b) radar profiles. Times specified are UTC.

Figure 6. Backscatter signatures of cirrus cloud deck (case study, June 26, 1996) averaged over the two flight segment intervals indicated; (a) lidar profile, (b) radar profiles. Times specified are UTC.

Figure 7. Range-resolved particle size retrievals for the cirrus case study depicted in Fig. 6. The putative uncertainty in size retrieval is denoted by the broken lines flanking the nominal retrieved r_e curve.

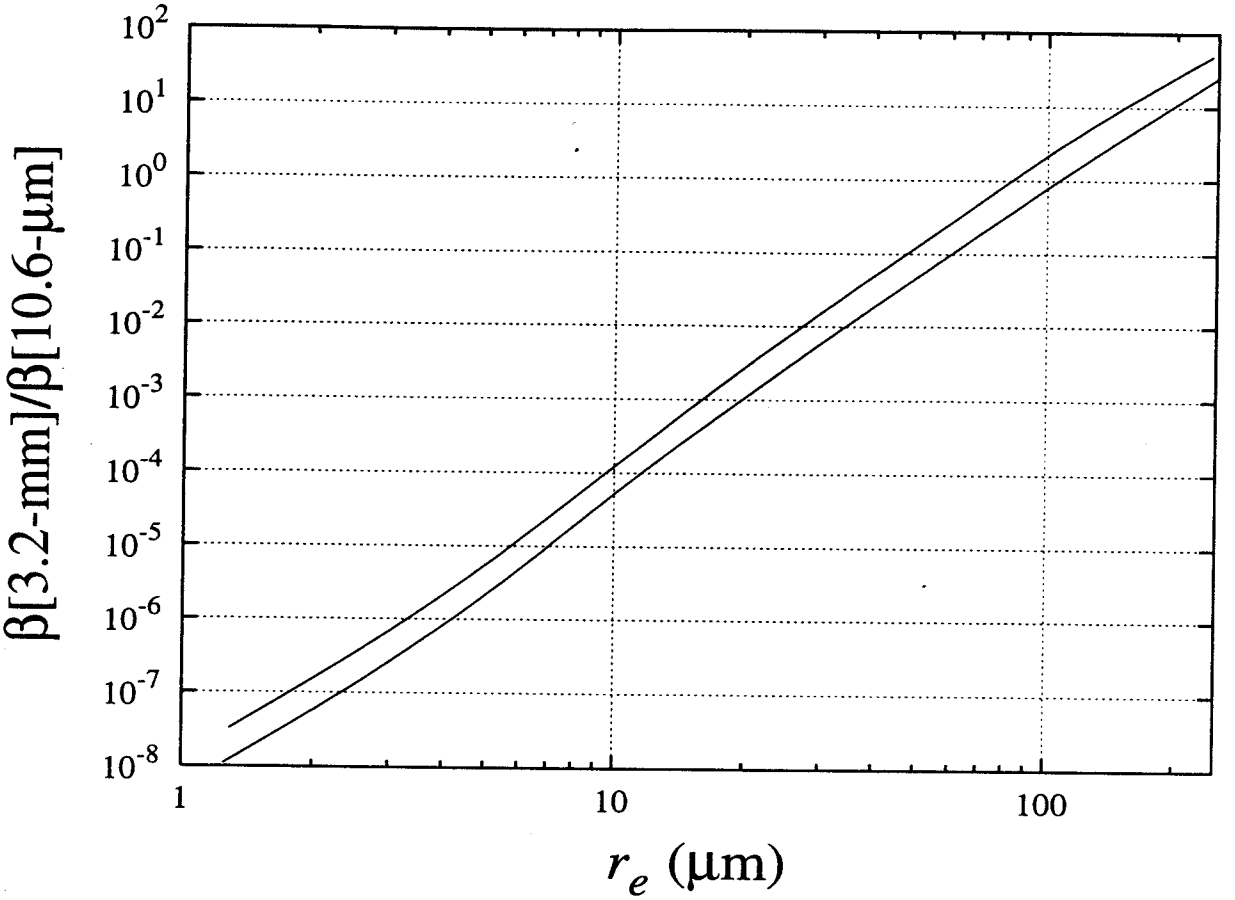

Figure 1. Mie theory simulations of 3.2-mm/10.6-μm backscatter ratio as a function of water droplet effective radius. The broad solution space bound by the two curves derives primarily from the variation in droplet size spectrum observed in natural non-precipitating water clouds.

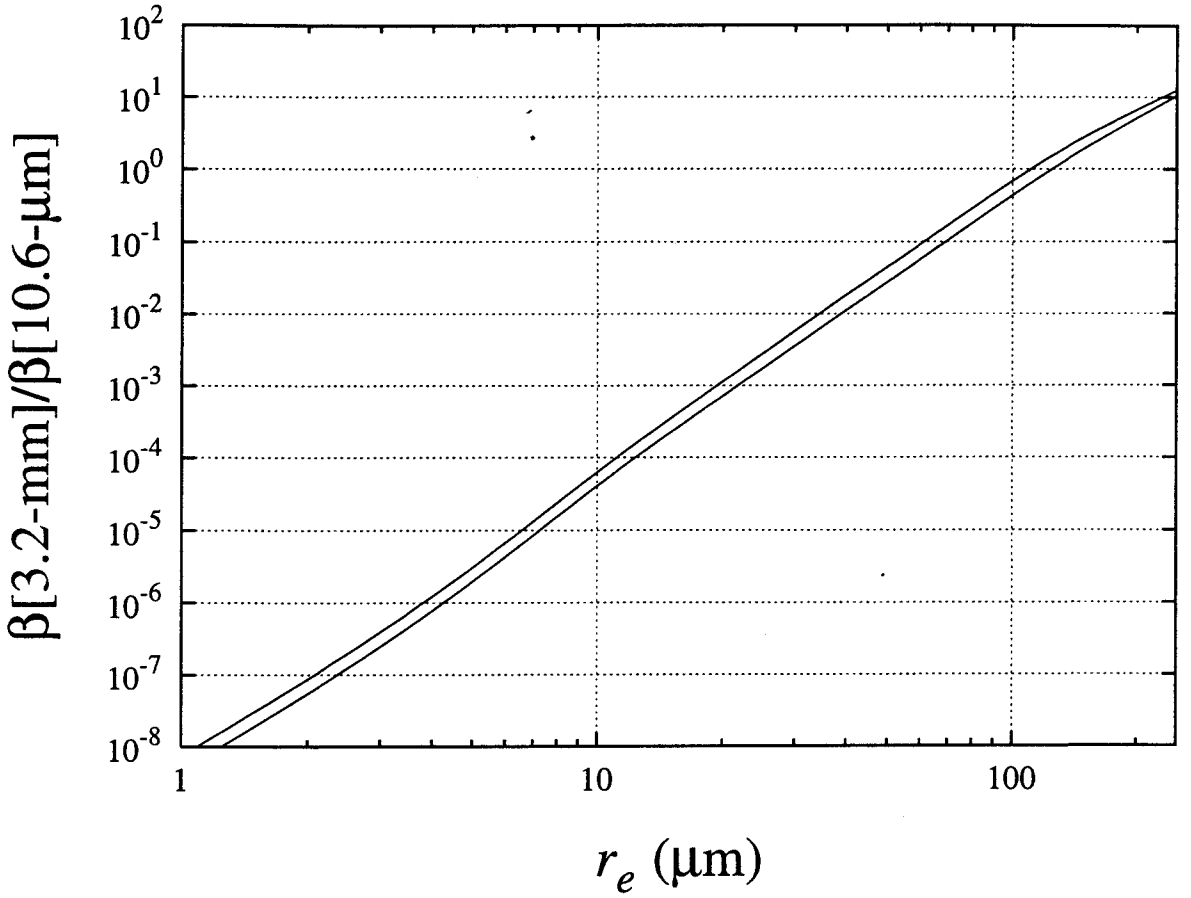

Figure 2. Mie theory simulations of 3.2-mm/10.6-μm backscatter ratio as a function of ice spherule effective radius. The broad solution space derives from the variation in particle size spectrum observed in natural cirrus clouds.

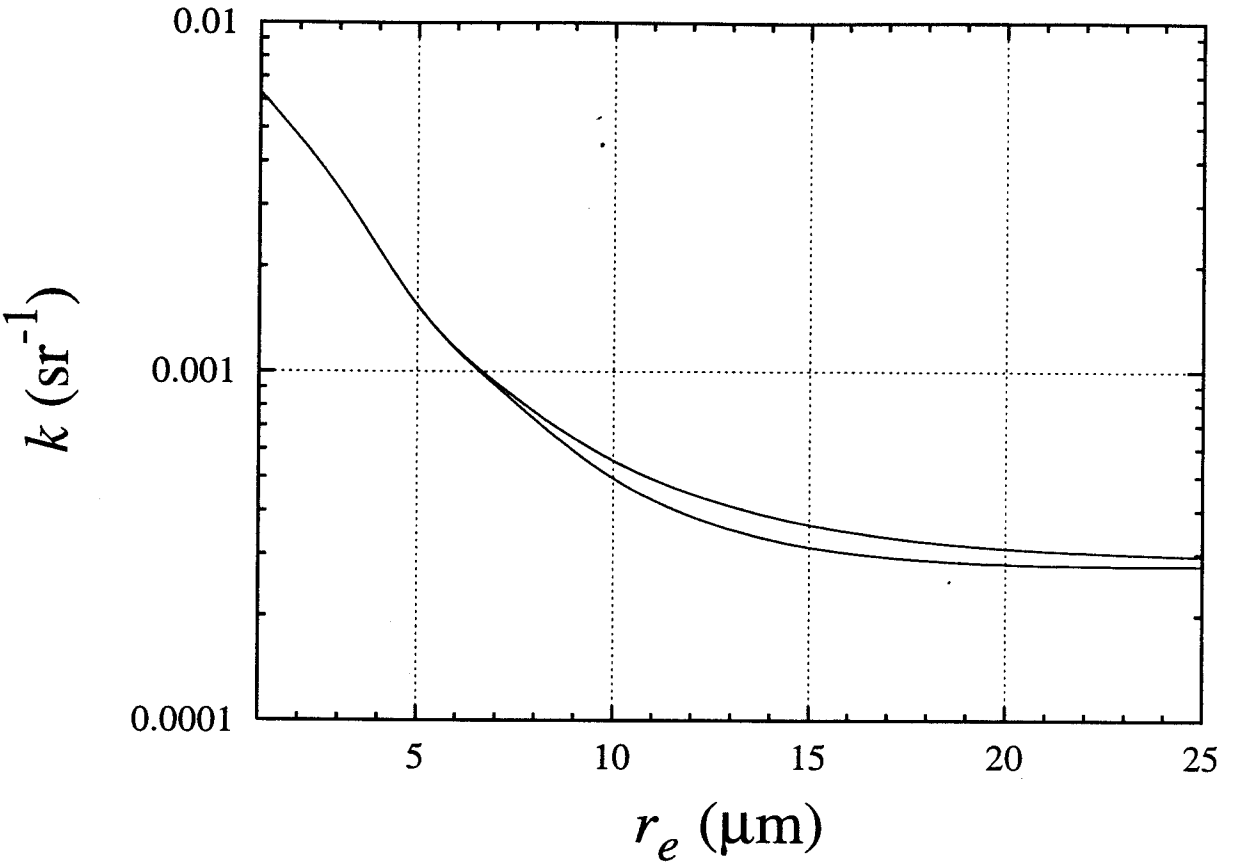

Figure 3. Dependence of cloud backscatter-to-extinction ratio at $\lambda = 10.6$ μm as a function of water droplet effective radius, as predicted by Mie theory. The bifurcate character of the relation denotes the uncertainty due to variations in the droplet size spectrum observed in natural non-precipitating water clouds.

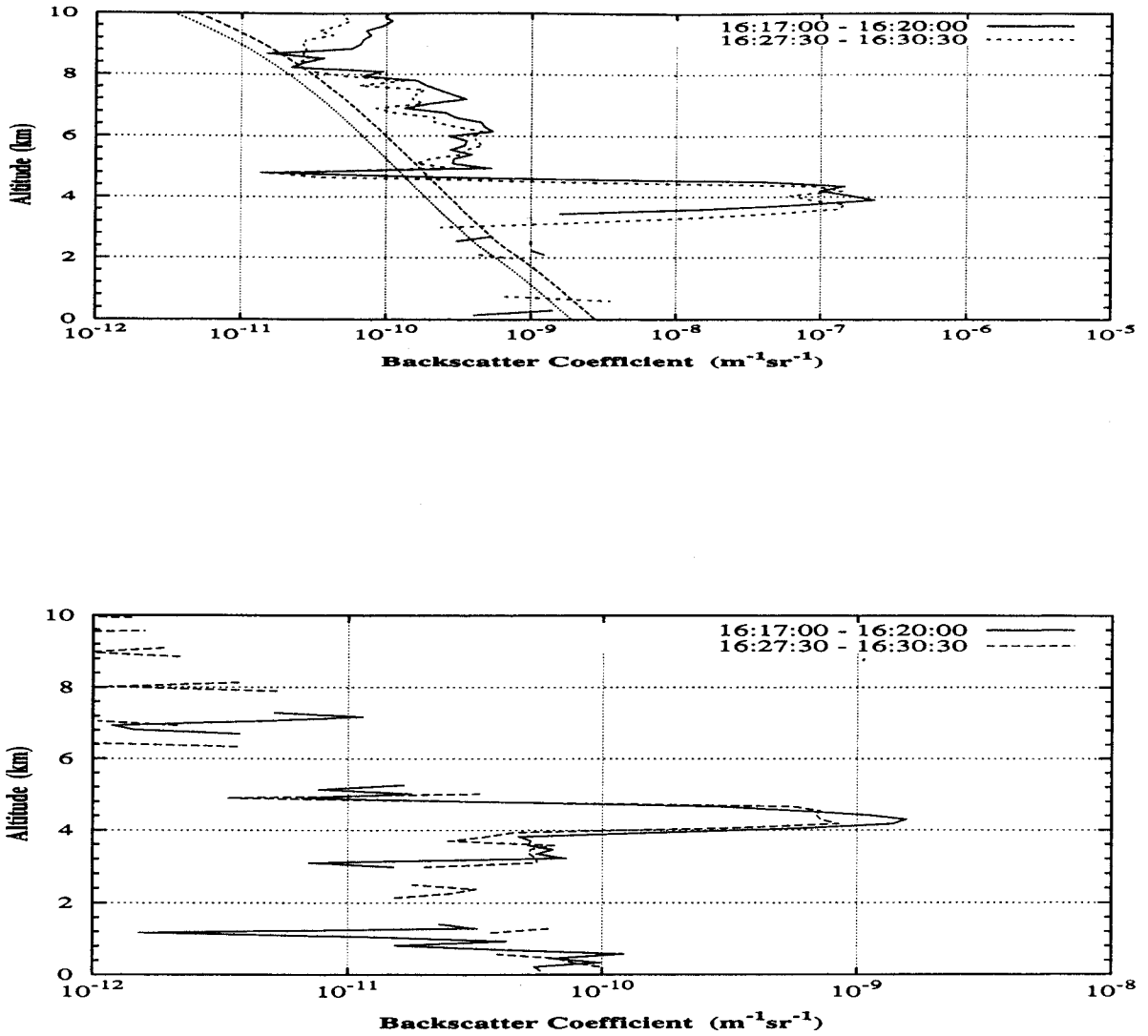

Figure 4. Backscatter signatures of altocumulus cloud deck (case study, June 24, 1996) averaged over the two flight segment intervals indicated; (a) lidar profiles, (b) radar profiles. Times specified are UTC.

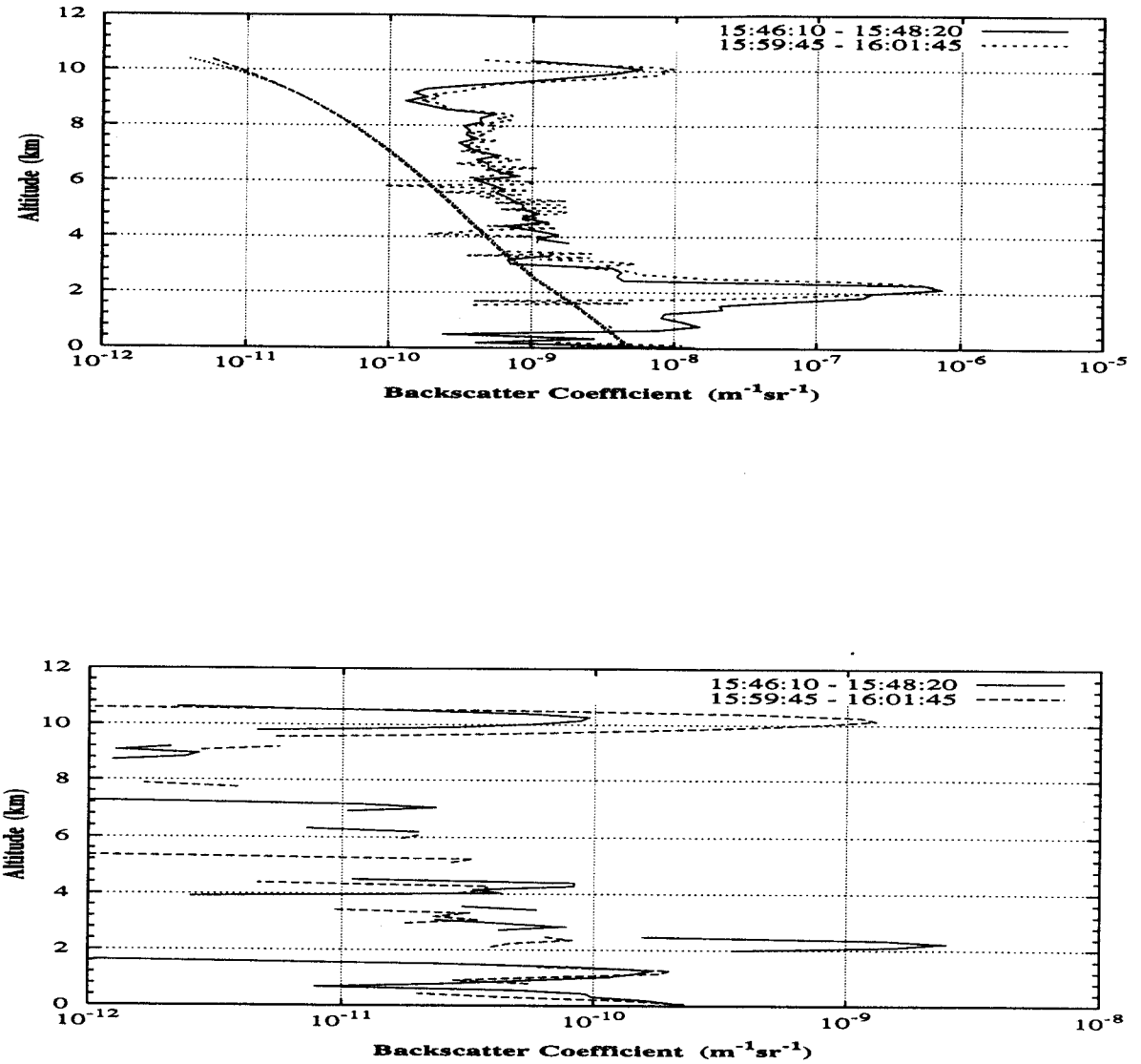

Figure 5. Backscatter signatures of stratocumulus cloud deck (case study, June 26, 1996) averaged over the two flight segment intervals indicated; (a) lidar profiles, (b) radar profiles. Times specified are UTC.

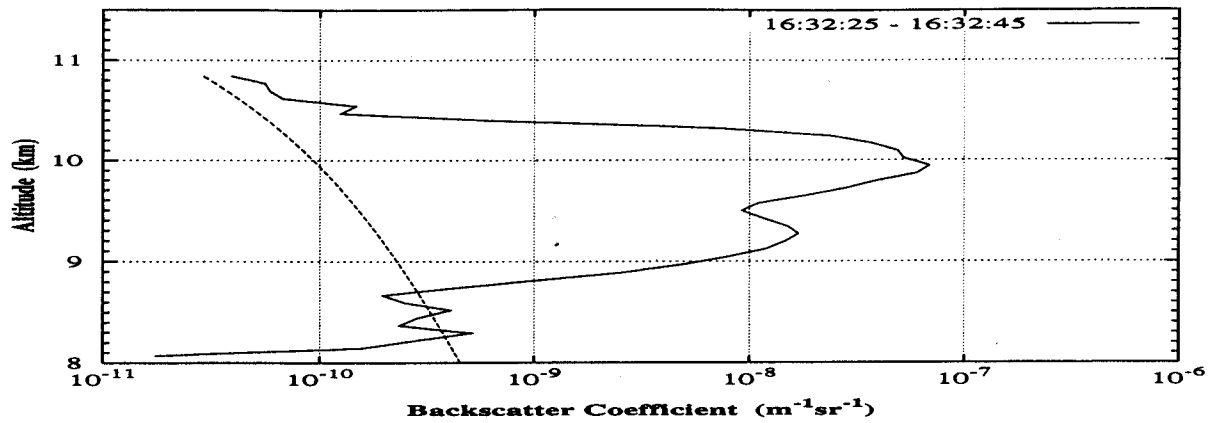

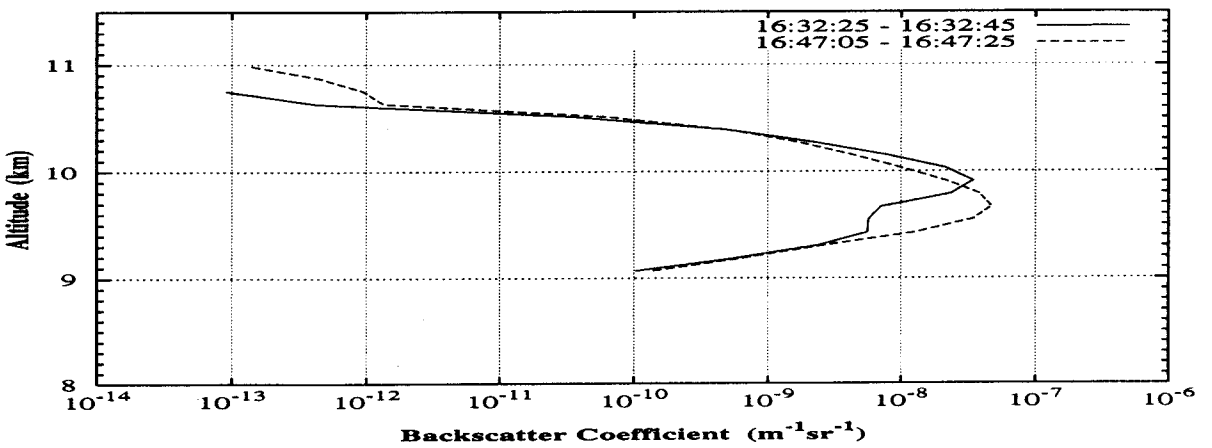

Figure 6. Backscatter signatures of cirrus cloud deck (case study, June 26, 1996) averaged over the two flight segment intervals indicated; (a) lidar profile, (b) radar profiles. Times specified are UTC.

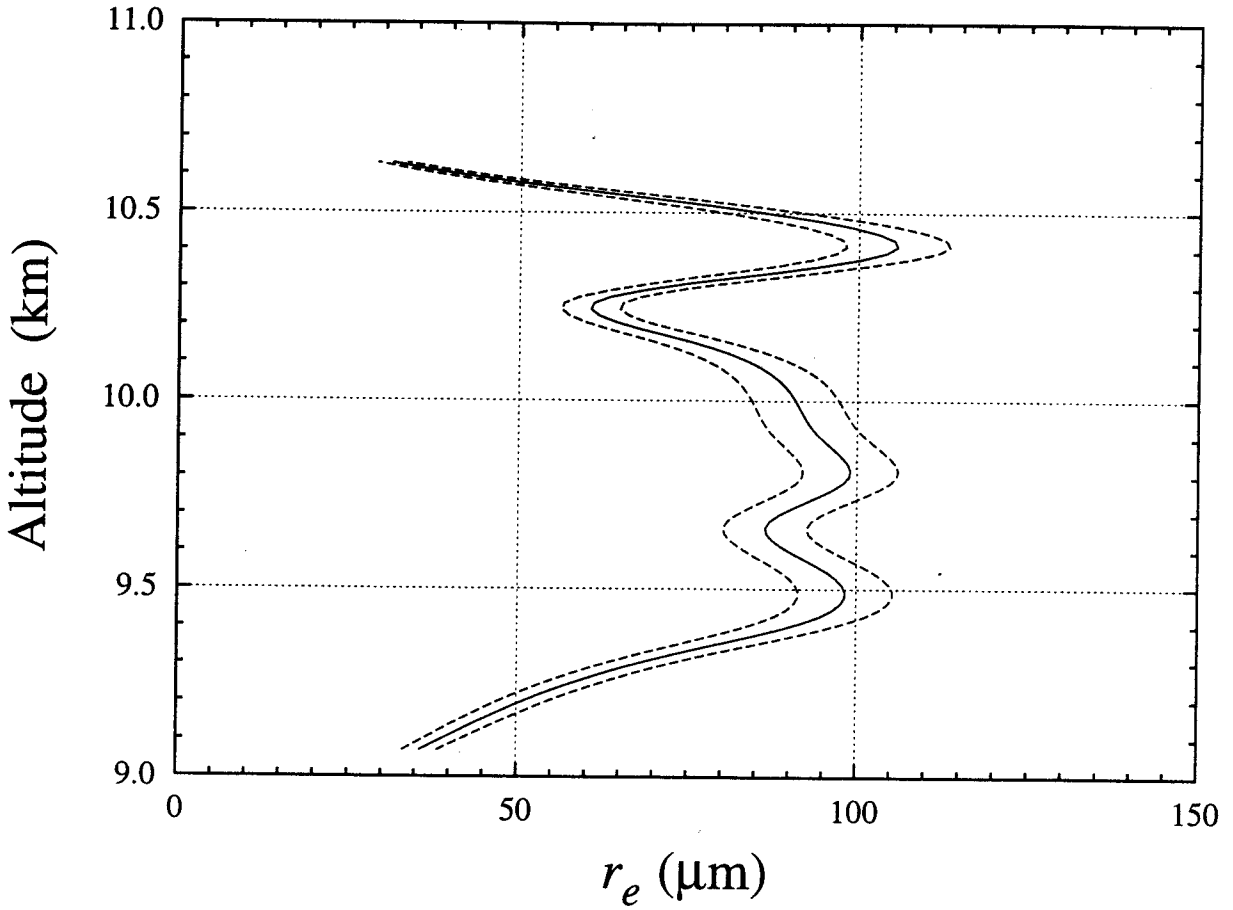

Figure 7. Range-resolved particle size retrievals for the cirrus case study depicted in Fig. 6. The putative uncertainty in size retrieval is denoted by the broken lines flanking the nominal retrieved r_e curve.